High-Frequency EPR Study of the Ferrous Ion in the Reduced Rubredoxin Model $[Fe(SPh)_4]^{2-}$

Michael J. Knapp,[†] J. Krzystek,[‡] Louis-Claude Brunel,[‡] and David N. Hendrickson*[,†]

Contribution from the Department of Chemistry and Biochemistry-0358, University of California at San Diego, La Jolla, California 92093, and Center for Interdisciplinary Magnetic Resonance, National High Magnetic Field Laboratory, Tallahassee, Florida 32310

Received August 20, 1999

High-frequency (94−371 GHz) EPR data are reported for powdered samples of $[PPh_4]_2[Fe(SPh)_4]$, an accurate model for the reduced site of rubredoxins. This is the first HFEPR investigation of an $S = 2$ ferrous complex, illustrating the utility of this technique for the investigation of integer-spin systems. A full-matrix diagonalization approach is used to simulate spectra over the 94−371 GHz frequency range, providing the spin-Hamiltonian parameters **g**, D, and E. It is observed that **g** is anisotropic, characterized by $g_x = g_y = 2.08$ and $g_z = 2.00$, and that $D = +5.84$ cm^{-1} and $E = +1.42$ cm^{-1}, where the uncertainty in each parameter is estimated as ±2%. The spin-Hamiltonian for $[PPh_4]_2[Fe(SPh)_4]$ is related to fundamental properties, such as the crystal-field splitting and the spin−orbit coupling of Fe^{2+}. It is shown that the conventional spin-Hamiltonian accurately represents the electronic structure of the Fe^{2+} ion in this molecule. Through a comparison with $Fe(SPh)_4(PPh_4)_2$, the zero-field splitting of the Fe^{2+} site in reduced rubredoxin is estimated to be $D = +5.3$ cm^{-1} and $E = +1.5$ cm^{-1}. This is one of the few HFEPR investigations of a rhombic, high-spin system; as such, it is a step toward the eventual investigation of similar Fe^{2+} sites in proteins.

Introduction

Iron plays an essential role in biological processes. In proteins, iron takes part in redox, oxygen transport, oxygen activation, and other chemical processes central to metabolic pathways.[1] The understanding of these metabolic processes has benefited from the study of small-molecule analogues, by virtue of their well-defined structures and ease of preparation. Iron−sulfur proteins and models have been studied for many years. The simplest iron−sulfur protein is rubredoxin (Rd), in which a single Fe atom is ligated by four cysteinyl ligands in a nearly tetrahedral arrangement. The Rd from *Clostridium pasteurianum* is the most widely studied of the class; it has a molecular mass of 6100 Da. The crystal structure of oxidized rubredoxin (Rd_{ox}) has been determined to 1.2 Å resolution,[2,3] revealing that the Fe^{3+} site of Rd lies very near the protein surface and has a solvent-exposed edge. Recently, the solution structure of reduced rubredoxin (Rd_{red}) was solved,[4] revealing that the position of Fe^{2+} relative to the protein backbone was virtually unchanged from that reported for Fe^{3+} in the crystal structure of Rd_{ox}. Also, EXAFS results[5,6] indicate that the average Fe−S(Cys) bond length of Rd_{ox} is 2.27 Å, while that of Rd_{red} is 2.32 Å, indicating that the overall geometries at the $Fe^{2+/3+}$ sites are very similar in both Rd_{ox} and Rd_{red}.

Rd undergoes electron-self-exchange (ESE) reactions on a very short time scale,[7] near the diffusion limit of 1×10^9 M^{-1} s^{-1}. The Fe^{3+} d orbital that accepts the electron upon reduction (d_{z^2}) is pointed directly at this water-exposed protein edge, suggesting that a simple outer-sphere electron-transfer (ET) mechanism may be operative, in contrast to the long-range ET thought to take place in many other proteins.[8,9]

Rd_{red} has been studied by a variety of spectroscopies. Optical spectroscopy[10] has revealed that the ligand-field splitting between the ^5E and $^5T_2$ states ($10Dq$) is approximately 6250 cm^{-1}, consistent with tetrahedral thiolate coordination. The spin Hamiltonian[11] incorporating axial (D) and rhombic (E) zero-field-splitting (zfs) terms, as well as the Zeeman interaction, is shown in eq 1. Mössbauer spectra[12−14] reveal that the ground

$$H = \mathbf{g}\beta\mathbf{SH} + D[\mathbf{S}_z^2 - {}^1/_3 S(S+1)] + E[\mathbf{S}_x^2 - \mathbf{S}_y^2] \quad (1)$$

state of the Fe^{2+} site is $^5A_1$ (d_{z^2} lowest) and is characterized by a rhombic, large zero-field splitting where $D \simeq +6$ cm^{-1} and $E/D = 0.28$.

[†] University of California at San Diego.
[‡] National High Magnetic Field Laboratory.

(1) Holm, R. H.; Kennepohl, P.; Solomon, E. I. *Chem. Rev.* **1996**, *96*, 2239−2314.
(2) Watenpaugh, K. D.; Sieker, L. C.; Jensen, L. H. *J. Mol. Biol.* **1979**, *131*, 509−522.
(3) Watenpaugh, K. D.; Sieker, L. C.; Jensen, L. H. *J. Mol. Biol.* **1980**, *138*, 615−633.
(4) Bertini, I.; Eidsness, M.; Liu, G.; Luchinat, C.; Rosato, A.; Scott, R. *J. Biol. Inorg. Chem.* **1998**, *3*, 401−410.
(5) Shulman, R.; Eisenberger, P.; Blumberg, W.; Stombaugh, N. *Proc. Natl. Acad. Sci. U.S.A.* **1975**, *72*, 4004.
(6) Shulman, R.; Eisenberger, P.; Teo, B.; Kincaid, B.; Brown, G. *J. Mol. Biol.* **1978**, *124*, 305.
(7) Jacks, C.; Bennett, L.; Raymond, W.; Lovenberg, W. *Proc. Natl. Acad. Sci. U.S.A.* **1974**, *71*, 1118.
(8) Bertini, I.; Gray, H.; Lippard, S.; Valentine, J. *Bioinorganic Chemistry*; University Science Books: Sausalito, CA, 1994.
(9) Gray, H. B.; Winkler, J. R. *Annu. Rev. Biochem.* **1996**, *65*, 537−561.
(10) Eaton, W.; Lovenberg, W. *J. Am. Chem. Soc.* **1970**, *92*, 7195−7198.
(11) Abragam, A.; Bleaney, B. *Electron Paramagnetic Resonance of Transition Metal Ions*; Dover: New York, 1970.
(12) Winkler, H.; Schultz, C.; Debrunner, P. *Phys. Lett.* **1979**, *69A*, 360.
(13) Schultz, C.; Debrunner, P. *J. Phys., Calloq.* **1976**, *37*, C6-153.
(14) Rao, K.; Evans, M.; Cammack, R.; Hall, D.; Thompson, C.; Jackson, P.; Johnson, C. *Biochem. J.* **1972**, *129*, 1063−1070.

10.1021/ic9910054 CCC: $19.00
Published on Web 12/31/1999

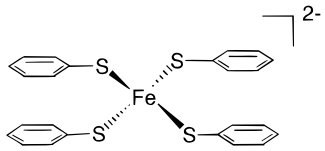

Figure 1. Schematic diagram of the $[Fe(SPh)_4]^{2-}$ anion, viewed down the molecular *Z* axis.

The model compound $[PPh_4]_2[Fe(SPh)_4]$ has been shown[15] to mimic the active site of Rd_{red}, in that its structural and electronic properties are quite similar. This compound has a tetrahedral arrangement of thiolate ligands that is tetragonally compressed about an approximate D_{2d} axis, in which the average Fe−S bond length is 2.35 Å. Figure 1 is a diagram of this cluster, in which the D_{2d} axis may be taken as coming out of the plane of the page. Mössbauer spectroscopy has shown that the ground state is $^5A_1$ (d_{z^2} lowest), while optical absorption spectroscopy indicated that the crystal field splitting $10Dq = 6000\ cm^{-1}$. The D_{2d} compression axis is likely the molecular *z* axis, that is, the likely principal axis of both the **g** and **D** tensors. Zero-field splitting has also been studied with far-infrared absorption[16] spectroscopy, where values of $D = +5.98\ cm^{-1}$ and $E = 1.42\ cm^{-1}$ have been determined. It is worth noting that another model complex for Rd_{red}, $[Fe(S_2\text{-}o\text{-}xyl)_2]^{2-}$, has been reported;[17] it also exhibits structural and electronic properties similar to those of the Rd_{red} site.

The distortion observed in tetrahedral ferrous complexes is crucial in determining the ground-state electronic structure.[18,19] An ideal tetrahedral geometry splits the five d orbitals to give an orbital doublet (^5E) ground state and a higher lying triplet ($^5T_2$) state. The orbital degeneracy of the ground ^5E state is broken by distortions from cubic symmetry. A distortion along a C_2 axis essentially determines the electronic structure, which in turn dictates the redox-active orbital for the $Fe^{2+/3+}$ couple. An elongation along the C_2 axis leads to an elongated tetragonal distortion, a negative zero-field splitting ($D < 0$), and a $^5B_1$ ground state in which the lowest energy d orbital is the $d_{x^2-y^2}$ orbital. A compression along the C_2 axis leads to a compressed tetragonal distortion, a positive zero-field splitting, and a $^5A_1$ ground state in which the lowest energy d orbital is the d_{z^2} orbital. Clearly, it is desirable to study $[Fe(SR)_4]^{2-}$ model complexes that have the $^5A_1$ ground state of Rd_{red}, such as $[PPh_4]_2[Fe(SPh)_4]$.

One notable study of the electronic structure of an Rd_{red} mimic is the investigation of the excited-state energies of $[Fe(2\text{-}(Ph)C_6H_4S)_4]^{2-}$ by the Solomon group.[20] This study revealed important details about the ferrous thiolate electronic structure, as probed by optical experiments aimed at determining the spin-forbidden charge-transfer energies. Foremost was the finding that there is extensive electronic relaxation upon the redox interconversion of $[Fe(SR)_4]^{2-/-}$. The complex $[Fe(2\text{-}(Ph)\text{-}C_6H_4S)_4]^{2-}$ was found to have a tetragonally elongated structure, and hence a negative *D* value, where the ground state is $^5B_1$. It is still necessary to explore the electronic structure of Rd_{red} mimics that possess the same ground state ($^5A_1$) as Rd_{red}.

Although the high-spin ($S = 2$) ferrous iron is a paramagnetic species, EPR studies of this ion are notably problematic. The main reason is the large zero-field splitting[19] ($D \approx 5-10\ cm^{-1}$) which either makes the allowed ($\Delta M_s = 1$) transitions between the spin sublevels inaccessible to the microwave energy quantum used in conventional EPR (ca. 0.3 cm^{-1} at X-band and ca. 1.2 cm^{-1} at Q-band frequencies) or makes them appear at fields much above those available in conventional EPR spectrometers. In such cases, high-frequency EPR (HFEPR, defined as $\nu \geq 95$ GHz) has been enormously successful for the study of non-Kramers transition metal ions having high spin and/or possessing large zfs. In particular, there have been two HFEPR papers reported[21,22] for high-spin Mn^{3+} as well as one HFEPR paper[23] for Cr^{2+}.

It is worth noting that ferrous iron, although a non-Kramers ion with typically large zfs, is not exactly "EPR silent" at conventional frequencies. This is because the significant rhombic term, *E*, both mixes the $m_s = |\pm 2\rangle$ zero-field energy levels, making transitions between them partially allowed, and brings those levels close in energy, making X- and Q-band EPR observations possible. An interesting technique[24] has been developed for the analysis of such spectra, but definitive information on non-Kramers spins is not always possible due to the low intensity and large line widths involved.

Many bioclusters, such as the P clusters and the FeMo-co of nitrogenase[25,26] and the mononuclear $Fe^{2+/3+}$ sites of Rd and SOD,[1] have ground states characterized by large and highly rhombic ($E/D > 0.1$) zero-field splittings, with the result being that conventional EPR techniques permit only indirect information on the magnitude of the zero-field splittings and **g** tensors. Further understanding of the electronic structure and reactivity of biologically relevant Fe clusters requires a more detailed knowledge of their magnetic properties. HFEPR at frequencies ranging from 95 to 670 GHz, as available at the National High Magnetic Field Laboratory, is expected to vastly augment this knowledge. Of particular importance is the availability of multiple frequencies, which will lead to a greater certainty in determining the magnitude of *g* and *D*.

An important aspect of performing HFEPR on randomly oriented samples of high-spin systems is the tendency of microcrystallites to orient with the magnetic field, which can be either beneficial or detrimental to the spectral information. Paramagnetic species whose ground state is characterized by a negative *D* have a particular tendency to orient along a single axis, often resulting in single-crystal-like spectra.[22,27−29] If the orientation is not perfect, however, effort must be made to ensure that the torquing effect does not influence the spectra and that

(15) Coucovanis, D.; Swenson, D.; Baenziger, N. C.; Murphy, C.; Holah, D. G.; Sfarnas, N.; Simopoulos, A.; Kostikas, A. *J. Am. Chem. Soc.* **1981**, *103*, 3350−3362.
(16) Champion, P. M.; Sievers, A. J. *J. Chem. Phys.* **1977**, *66*, 1819−1825.
(17) Lane, R.; Ibers, J.; Frankel, R.; Papaefthymiou, G.; Holm, R. *J. Am. Chem. Soc.* **1977**, *99*, 84−98.
(18) Hartmann-Boutron, F.; Imbert, P. *J. Appl. Phys.* **1968**, *39*, 775−785.
(19) Solomon, E. I.; Pavel, E. G.; Loeb, K. E.; Campochiaro, C. *Coord. Chem. Rev.* **1995**, *144*, 369−460.
(20) Gebhard, M. S.; Koch, S. A.; Millar, M.; Devlin, F. J.; Stephens, P. J.; Solomon, E. I. *J. Am. Chem. Soc.* **1991**, *113*, 1640−1649.
(21) Barra, A. L.; Gatteschi, D.; Sessoli, R.; Abbati, G. L.; Cornia, A.; Fabretti, A. C.; Uytterhoeven, M. G. *Angew. Chem., Int. Ed. Engl.* **1997**, *36*, 2329−2331.
(22) Goldberg, D. P.; Telser, J.; Krzystek, J.; Montalban, A. G.; Brunel, L. C.; Barrett, A. G. M.; Hoffman, B. M. *J. Am. Chem. Soc.* **1997**, *119*, 8722−8723.
(23) Telser, J.; Pardi, L.; Krzystek, J.; Brunel, L. C. *Inorg. Chem.* **1998**, *37*, 5769−5775.
(24) Hendrich, M. P.; Debrunner, P. G. *Biophys. J.* **1989**, *56*, 489−506.
(25) Lindahl, P. A.; Day, E. P.; Kent, T. A.; Orme-Johnson, W. H.; Munck, E. *J. Biol. Chem.* **1985**, *260*, 11160.
(26) Surerus, K. K.; Hendrich, M. P.; Christie, P. D.; Rottgardt, D.; Orme-Johnson, W. H.; Munck, E. *J. Am. Chem. Soc.* **1992**, *114*, 8579−8590.
(27) Aubin, S. M. J.; Dilley, N. R.; Pardi, L.; Krzystek, J.; Wemple, M. W.; Brunel, L. C.; Maple, M. B.; Christou, G.; Hendrickson, D. N. *J. Am. Chem. Soc.* **1998**, *120*, 4991−5004.
(28) Barra, A. L.; Caneschi, A.; Gatteschi, D.; Sessoli, R. *J. Magn. Magn. Mater.* **1998**, *177*, 709−710.
(29) Barra, A. L.; Brunel, L.-C.; Gatteschi, D.; Pardi, L.; Sessoli, R. *Acc. Chem. Res.* **1998**, *31*, 460−466.

the distribution of molecules is truly random. One way to do so is to perform the HFEPR experiment on a frozen solution as was done with success on water solutions of Cr^{2+} salts.[23] The latter result is particularly important since it demonstrates that it is possible to perform HFEPR on water solutions, the medium expected for future studies of biological systems. Another way of obtaining a random distribution of molecules is to immobilize a microcrystalline sample in a solid a matrix. This work describes the HFEPR study of microcrystalline $[PPh_4]_2[Fe(SPh)_4]$ immobilized in a KBr pellet, undertaken to characterize the ground-state electronic properties of this analogue of the Rd_{red} site. It should be mentioned that all high-spin non-Kramers species studied so far were characterized by $D < 0$, whereas this complex is characterized by $D > 0$. This is only the fourth $S = 2$ spin system investigated by HFEPR[21−23] and the first high-spin system that is biologically relevant. Randomly oriented samples were used to further our understanding of powder patterns in systems characterized by large zfs. This forms a first step toward the ultimate goal of applying HFEPR to high-spin protein sites.

Experimental Section

The compound $[PPh_4]_2[Fe(SPh)_4]$ was prepared by published methods[20] using commercially available reagents. HFEPR samples were prepared by grinding $[PPh_4]_2[Fe(SPh)_4]$ with KBr under an inert atmosphere and then forming a solid pellet.[30]

HFEPR experiments were performed at the National High Magnetic Field Laboratory, Tallahasee, FL. A superconducting Oxford Instruments magnet system (field strength 17 T) capable of high sweep rates (up to 0.5 T/min) was used. The microwave sources were two Gunn diodes of 95 and 110 GHz nominal frequencies. Harmonic generators permitted experiments at nominal frequencies of $n \times 95$ and $n \times 110$ GHz, where n is an integer from 2 to 4. Spectra run at higher frequencies have reduced signal-to-noise ratios since the microwave power falls off rapidly at the higher harmonics. High-pass filters were used to eliminate lower harmonics; however, higher harmonics frequently were evident in the experimental spectra. Phase detection with a magnetic field modulation was employed. A liquid-helium-cooled InSb bolometer from QMC Instruments was used as the detector. Further details will be described in a forthcoming paper.[31]

The experiments described in this report were performed using a single-pass transmission setup. This configuration is characterized by a lower sensitivity than the one using a resonator in terms of absolute number of spins/G detectable. However, due to much larger sample volume (up to 0.5 mL) available in the transmission configuration and the fact that at high frequencies only multimode resonators of relatively low conversion factors can be used, the difference in concentration sensitivity between the two versions is lower than one might expect, approximately 1 order of magnitude.[32] The single-pass setup has the great advantage of operation over a broad range of frequencies. As shown in this paper, this multifrequency capability is of great help in identifying and following EPR transitions in the complicated spectra that characterize integer-spin complexes.

EPR spectra were simulated using the computer program SIM.[33−35] SIM calculates the energy levels of the spin state by full-matrix diagonalization of the spin Hamiltonian. The standard spin Hamiltonian was used (eq 1), in which it was assumed that **D** and **g** are collinear. Resonant fields were determined by the energy differences between levels, with the simulated line shape determined by considering both transition probabilities and Boltzmann population differences between the energy levels. The output from SIM was also used to determine the angular dependence of resonant fields.

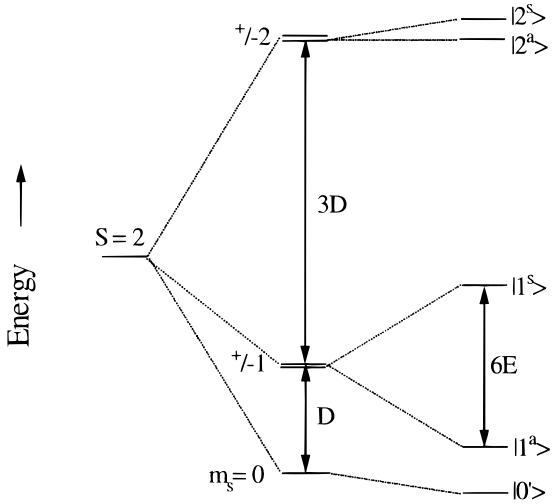

Figure 2. An $S = 2$ state undergoing axial (D) and rhombic (E) zero-field splitting. The eigenfunctions are given in eq 2.

Results and Discussion

HFEPR Spectroscopic Measurements. An $S = 2$ spin system has five degenerate energy levels ($M_s = \pm 2, \pm 1, 0$) in the absence of zero-field-splitting effects (Figure 2, left). The degeneracy of these levels is broken in the presence of zfs, such as caused by spin−orbit coupling, according to the spin Hamiltonian in eq 1. A purely axial zfs leads to the splitting indicated in the middle of Figure 2, while the effect of a rhombic zfs ($E \neq 0$) leads to the splitting illustrated on the right-hand side of this figure. The labels for the energy levels of Figure 2 are strictly accurate only at very low magnetic fields; however, the low-field labels will be used throughout this paper for simplicity. The composition of the zero-field eigenfunctions of eq 1 is as follows:[24]

$$|2^s\rangle = [{}^1/_2(1 + D/(D^2 + 3E^2)^{1/2})]^{1/2}(|+2\rangle + |-2\rangle)/2^{1/2} + [{}^1/_2(1 - D/(D^2 + 3E^2)^{1/2})]^{1/2}|0\rangle \quad (2a)$$

$$|2^a\rangle = (|+2\rangle - |-2\rangle)/2^{1/2} \quad (2b)$$

$$|1^s\rangle = (|+1\rangle + |-1\rangle)/2^{1/2} \quad (2c)$$

$$|1^a\rangle = (|+1\rangle - |-1\rangle)/2^{1/2} \quad (2d)$$

$$|0'\rangle = [{}^1/_2(1 - D/(D^2 + 3E^2)^{1/2})]^{1/2}(|+2\rangle + |-2\rangle)/2^{1/2} - [{}^1/_2(1 + D/(D^2 + 3E^2)^{1/2})]^{1/2}|0\rangle \quad (2e)$$

HFEPR spectra were collected on a ground sample of $[PPh_4]_2[Fe(SPh)_4]$ in a KBr pellet at 20 K over the nominal 94−371 GHz frequency range; the data are shown in Figure 3. The EPR signal is plotted for each frequency as a function of the applied magnetic field. The spectra are quite complicated, with many features observable at a few frequencies that disappear at higher and/or lower frequencies. At the lower frequencies (95−216 GHz), there is one feature at low field that moves to higher field as frequency increases, from 0.49 T at 95 GHz to 1.83 T at 216 GHz. At the higher frequencies, this feature disappears. There is one other feature evident at lower frequencies which

(30) Knapp, M.; Krzystek, J.; Brunel, L.-C.; Hendrickson, D. *Inorg. Chem.* **1999**, *38*, 3321−3328.
(31) Hassan, A.; Pardi, L. A.; Krzystek, J.; Sienkiewicz, A.; Goy, P.; Rohrer, M.; Brunel, L. C. Submitted for publication.
(32) Rohrer, M.; Krzystek, J.; Williams, V.; Brunel, L.-C. *Meas. Sci. Technol.* **1999**, *10*, 275−284.
(33) Glerup, J.; Weihe, H. *Acta Chem. Scand.* **1991**, *45*, 444−448.
(34) Glerup, J.; Weihe, H. *Inorg. Chem.* **1997**, *36*, 2816−2819.
(35) Jacobsen, C. J. H.; Pedersen, E.; Villadsen, J.; Weihe, H. *Inorg. Chem.* **1993**, *32*, 1216−1221.

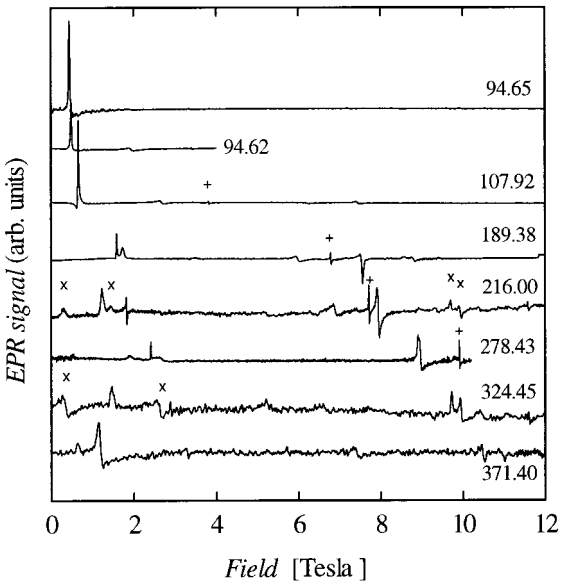

Figure 3. HFEPR spectra for a sample of $[PPh_4]_2[Fe(SPh)_4]$ pressed into a KBr pellet collected at 20 K in the 94−324 GHz frequency range. Each spectrum is labeled with its nominal frequency. Features marked with an "×" arise from a higher harmonic of the fundamental frequency, and "+" indicates a $g = 2$ impurity.

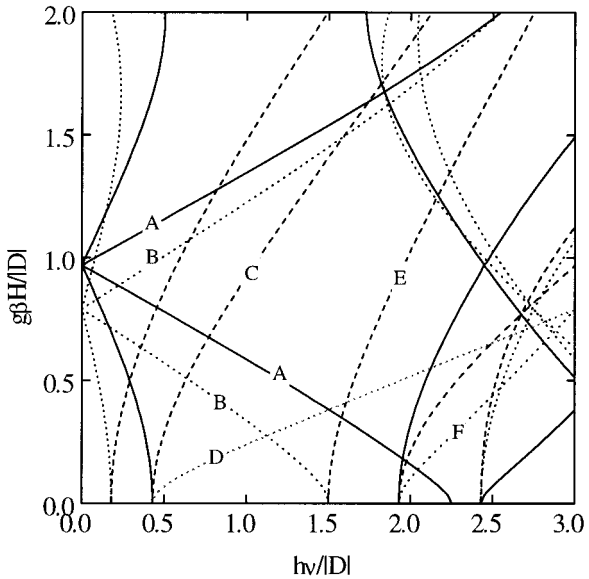

Figure 4. Plot of Zeeman energy vs microwave energy, normalized by D, for an $S = 2$ state characterized by $g = 2$ and rhombicity $E/D = 0.25$. The plotted lines indicate the resonant field position (H) as a function of the microwave frequency, ν, for transitions which have a $\Delta M_s = \pm 1$ component under either low-field or high-field conditions. The applied magnetic field is parallel to either the X axis (dashed line), Y axis (dotted line), or Z axis (solid line).

moves from 1.92 T at 95 GHz to 6.89 T at 216 GHz; it seems to merge in with an intense feature at 8.96 T in the 278 GHz spectrum. At higher frequencies, several features are evident in the 0−4 T range, whose frequency-dependent behavior is not clear upon initial inspection. It appears that several resonances just begin to be observable at these higher frequencies by virtue of the larger microwave quanta (ca. 10 cm^{-1}). In contrast to the confusion at lower fields, at higher fields there are two sets of signals that move from 6.25 and 7.43 T at 108 GHz to 10.48 and 11.01 T at 371 GHz. In addition, there is a sharp line that appears near $g = 2$, the resonant field of the free electron, in all the spectra, which is denoted by a "+". This feature is of unknown origin but might originate from a small organic radical impurity, or perhaps it is due to a multiple-quantum transition. Further research is needed on this transition.

In an axial system, it would be expected that the dominant features would have a frequency variation that approached that of the $g = 2$ resonance[23] and moved to higher field as the frequency increased. Clearly, the dominant features do not have such a frequency dependence. This system is not a simple axial system.

EPR selection rules dictate that transitions between energy levels are allowed only if the condition $\Delta M_s = \pm 1$ is met.[36] A qualitative understanding of why certain transitions disappear at either high- or low-fields may be obtained from this simple "allowedness" argument. Transitions between energy levels gain intensity by virtue of each energy level having some component of M_s states such that the transition has some $\Delta M_s = \pm 1$ character. As the composition of each energy level changes in response to the magnetic field, the "allowedness" of many transitions changes dramatically, from highly allowed at one value of the field to totally forbidden at higher (or lower) fields. This is the reason most resonances in the HFEPR spectra of $[PPh_4]_2[Fe(SPh)_4]$ are observed at only a few frequencies. As this complex is an integer-spin complex experiencing significant rhombic zfs, the energy levels result from a mixture of several M_s states; this degree of mixing and the composition of each energy level are quite field dependent, leading to a transition being allowed at certain values of the magnetic field (and hence certain frequencies) but only very weakly allowed (if at all) at other field positions. For example, the two levels denoted $|1^a\rangle$ and $|1^s\rangle$ (see Figure 2) have the zero-field compositions given in eq 2. Clearly, at low fields there is no $\Delta M_s = 1$ component in a transition between these two levels. At the strong field limit ($D \ll g\beta H$) for a rhombic system ($E/D = 0.25$) the composition of these levels differs depending upon which molecular axis (X, Y, or Z) is parallel to the magnetic field. When the magnetic field is parallel to the Y axis, the energy level derived from $|1^s\rangle$ has the high-field composition of dominantly $|-1\rangle$, while the energy level derived from $|1^a\rangle$ is dominantly $|0\rangle$ at high field. Clearly, at high fields, there is a $\Delta M_s = 1$ component to transitions between the $|1^s\rangle$ and $|1^a\rangle$ energy levels. The allowedness of the transition between these levels will change as the magnetic field changes. Unraveling the electronic structure of such a system is not possible from simple inspection of the EPR spectra, as clearly the zero-field splitting is of the same order of magnitude as the Zeeman splitting under all accessible frequencies and the zfs is appreciably rhombic. Fortunately, the zfs of $[PPh_4]_2[Fe(SPh)_4]$ has been investigated by a variety of other techniques,[15,16] indicating that $D \simeq +6$ cm^{-1} and $E/D \simeq 0.25$.

Theoretical resonant field vs frequency diagrams were used to check the reported rhombicity and D values and to identify spectral features. The analytical expressions of Baranowski et al.[37] were used to generate the resonant field vs frequency diagrams for various values of E/D. These expressions provide the energy of the five energy levels along each of the X, Y, and Z axes of **g**, assuming that both **g** and **D** are collinear. The resonant field vs frequency diagram for $E/D = 0.25$ is shown in Figure 4. In this figure, the resonant field is plotted in the form of Zeeman energy ($g\beta H$) normalized by the axial zfs

(36) Weltner, W., Jr. *Magnetic Atoms and Molecules*; Scientific and Academic Editions: New York, 1983.

(37) Baranowski, J.; Cukierda, T.; Jezowska-Trzebiatowska, B.; Kozlowski, H. *J. Magn. Reson.* **1979**, *33*, 585−593.

parameter D; this is plotted as a function of the transition energy ($h\nu = \Delta E$) which is also normalized by D. Each curve indicates the field/frequency response of a transition that has some $\Delta M_s = 1$ character at either high field or zero field; transitions with no $\Delta M_s = 1$ character were not considered. For this reason, there are numerous transitions that may be only weakly allowed and therefore unobservable in powder samples.

If a vertical line is drawn at $h\nu/D = 1$, this reveals the approximate resonant position expected when $h\nu = D$ for each of the allowed transitions. It can be seen that there should be three transitions at low fields ($g\beta H/D = 0.2-0.6$) and four transitions at higher fields ($g\beta H/D = 1.0-1.5$). In fact, this pattern of resonances is essentially observed at 189 GHz ($h\nu = 6.33$ cm^{-1}), where three transitions are observed in the 0−4 T range and three transitions are observed in the 6−11 T range (Figure 3). Thus, the HFEPR spectra are consistent with $D \simeq +6$ cm^{-1} and $E/D \simeq 0.25$. In this manner, the two EPR features observed at high fields at most frequencies were identified as likely arising from the $|1^s\rangle \rightarrow |2^a\rangle$ (line A in Figure 4) and $|1^a\rangle \rightarrow |1^s\rangle$ (line B in Figure 4) transitions. Other frequencies ($h\nu/D$ values) may be explored in a similar fashion. This provides a qualitative way to identify the various dominant spectral features without resorting to simulation; furthermore, it provides a quick check on the magnitude of D derived from other sources, such as Mössbauer data, which give less precise values of D and E than EPR data.

Far-Infrared Resonances in Zero-Field. The strength of EPR is that very precise measurements of both **g** and **D** are possible; however, this is also a weakness, as uncertainties in **g** will lead to uncertainties in **D** and vice versa. If it were possible to obtain the zfs parameters without the complication of Zeeman splitting, greater accuracy in these parameters would be possible. Fortunately, $[PPh_4]_2[Fe(SPh)_4]$ has been studied by far-IR absorption spectroscopy.[16] These far-IR measurements were carried out in zero applied field and provide an accurate measurement of the energies of the five M_s levels, according to the Hamiltonian in eq 3. Those workers[16] quoted zfs parameters

$$H = D[S_z^2 - {}^1/_3 S(S+1)] + E[S_x^2 - S_y^2] \qquad (3)$$

which they derived only from the energies of the three lowest levels (see Figure 2) by a simple approximation and did not consider the energies of the two uppermost levels. In this manner, there was a discrepancy between the observed and calculated transitions involving the two uppermost levels. It was suggested[16] that higher-order zfs terms might be the origin of this discrepancy.

Far-IR transition energies were refit using analytical expressions of Baranowski et al.[37] to better account for the entire data set and to obtain accurate zfs parameters. The energies of the transitions, both those reported and the fit values, are listed in Table 1. To fit the far-IR data, a spreadsheet was constructed, and then D and E were stepped through 0.01 cm^{-1} increments. The error was defined as the sum of squares difference between the reported far-IR transition energy and the calculated transition energy for each of the six reported transitions. The error surface is shown as a contour plot in Figure 5, in which isovalue error curves are displayed as a functions of E and D. Clearly, both E and D are well defined by the far-IR data; the best fit was obtained with $D = 5.82 \pm 0.04$ cm^{-1}, and $E = 1.44 \pm 0.02$ cm^{-1}, for a rhombicity of $E/D = 0.24-0.25$. We note that these best-fit values are slightly different from those reported earlier; specifically, D is some 0.2 cm^{-1} smaller. Nevertheless, this small difference led to appreciable differences in the EPR simulations.

Table 1. Zero-Field Transitions of $[PPh_4]_2[Fe(SPh)_4]$[a]

transition	exptl (far-IR data[b]), cm^{-1}	calcd, cm^{-1}		
		c	*d*	*e*
$\|0'\rangle \rightarrow \|1^a\rangle$	2.7	2.69	2.52	2.57
$\|0'\rangle \rightarrow \|1^s\rangle$	11.2	11.21	11.16	11.09
$\|1^a\rangle \rightarrow \|1^s\rangle$	8.6	8.52	8.64	8.52
$\|1^a\rangle \rightarrow \|2^a\rangle$	21.8	22.20	21.78	21.78
$\|1^s\rangle \rightarrow \|2^a\rangle$	13.1	13.68	13.14	13.26
$\|1^s\rangle \rightarrow \|2^s\rangle$	14.1	14.65	14.16	14.25

[a] The experimental points are from far-IR measurements, and the calculated energies are from analytical solutions for the indicated values of D and E. [b] Data from *J. Chem. Phys.* **1977**, *66*, 1819−1825. All transitions have an estimated uncertainty of ±0.2 cm^{-1}. [c] Calculated from analytical expressions for $D = +5.98$ cm^{-1} and $E = 1.42$ cm^{-1}. [d] Calculated from analytical expressions for $D = +5.82$ cm^{-1} and $E = 1.44$ cm^{-1}. [e] Calculated from analytical expressions for $D = +5.84$ cm^{-1} and $E = 1.42$ cm^{-1}.

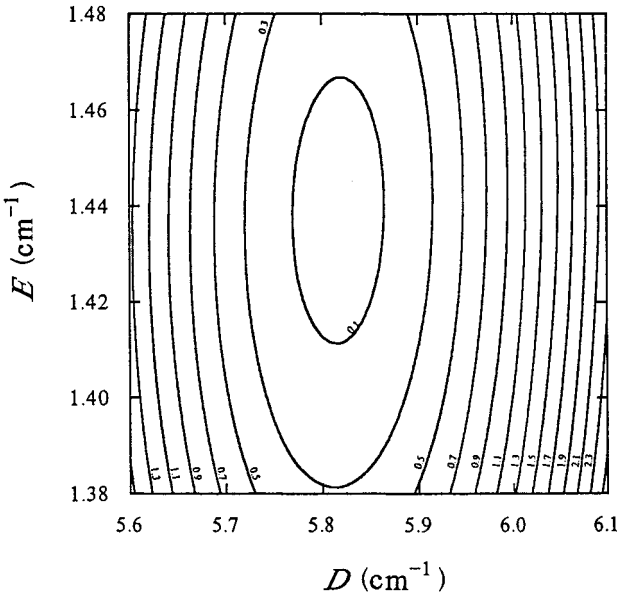

Figure 5. Isoerror curves as functions of D and E from fitting the far-IR energies to theoretical equations. The best fit is characterized by $D = +5.82 \pm 0.06$ cm^{-1} and $E = +1.44 \pm 0.02$ cm^{-1}.

Finally, the spin Hamiltonian (eq 3) incorporating only axial and rhombic zfs terms adequately described the ground-state of $[PPh_4]_2[Fe(SPh)_4]$; higher order zfs terms are not necessary, as was previously suggested.[16]

Simulations of the HFEPR Spectra. Simulations were performed using the zfs parameters from the best-fit region of the far-IR data set. Very quickly, it became apparent that an anisotropic **g** was required, with $g_z \simeq 2$ and g_x, $g_y \simeq 2.1$. Trial and error led to the "best" simulations, which incorporated the following parameters: $g_x = g_y = 2.08$, $g_z = 2.00$, $D = +5.84$ cm^{-1}, $E = +1.42$ cm^{-1}. The estimated uncertainty in each parameter is ±2%. Three representative simulations are shown in Figures 6 and 7. The 189.38 GHz spectrum (A), with a simulation (B), is shown in Figure 6. There is excellent agreement between the observed and simulated resonant fields and intensities. The lowest field features, at 1.6 and 1.8 T, are split in the experimental spectrum, whereas simulations indicate that the two features are unresolved. The feature at 1.6 T may be a signal from an impurity such as Fe^{3+}, as it is quite sharp; however, its field-frequency behavior matches that predicted for a genuine transition arising from the Fe^{2+} sample. The spectrum recorded at a nominal frequency of 324.45 GHz is shown in Figure 7, with two simulations. The first simulation was performed at a frequency of 324.45 GHz (Figure 7B) and

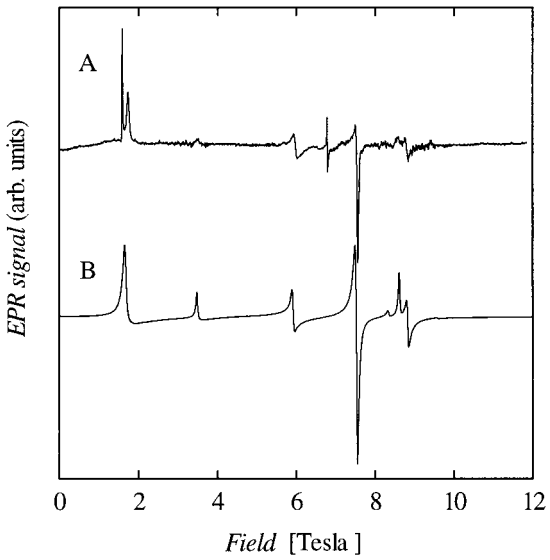

Figure 6. (A) HFEPR spectrum for a sample of $[PPh_4]_2[Fe(SPh)_4]$ pressed into a KBr pellet collected at 20 K and a frequency of 189.38 GHz. (B) Simulated 189.38 GHz HFEPR spectrum using the following parameters: $g_x = g_y = 2.08$, $g_z = 2.00$, $D = +5.84$ cm^{-1}, $E = +1.42$ cm^{-1}.

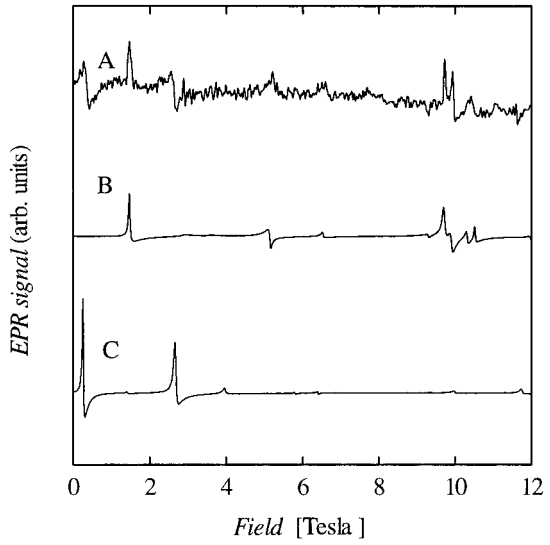

Figure 7. (A) HFEPR spectrum for a sample of $[PPh_4]_2[Fe(SPh)_4]$ pressed into a KBr pellet collected at 20 K and a frequency of 324.45 GHz. (B) Simulated 324.45 GHz HFEPR spectrum using the following parameters: $g_x = g_y = 2.08$, $g_z = 2.00$, $D = +5.84$ cm^{-1}, $E = +1.42$ cm^{-1}. (C) Simulated 432.60 GHz HFEPR spectrum using the following parameters: $g_x = g_y = 2.08$, $g_z = 2.00$, $D = +5.84$ cm^{-1}, $E = +1.42$ cm^{-1}.

accounts for most of the experimental features, such as the sharp signal at 1.5 T and the split feature near 9.8 T. However, as stated in the Experimental Section, higher harmonics produced by the frequency multiplier can pass through; in this case, radiation from the fourth harmonic of the 110 GHz source (432.60 GHz) passes through. A simulation at this higher frequency (Figure 7C) is also shown, and as can be seen, it accounts for the two remaining features at 0.4 and 2.6 T.

The observed features which correspond to axial resonances (*H*||*X*, *Y*, or *Z*) are plotted in Figure 8, together with the simulated features, in the form of a resonant field vs frequency diagram. There is excellent correspondence between the calculated and the observed resonant field positions. From a comparison with Figure 4, assigning the features is straightforward. The two branches marked "A" arise from a resonance along the molecular

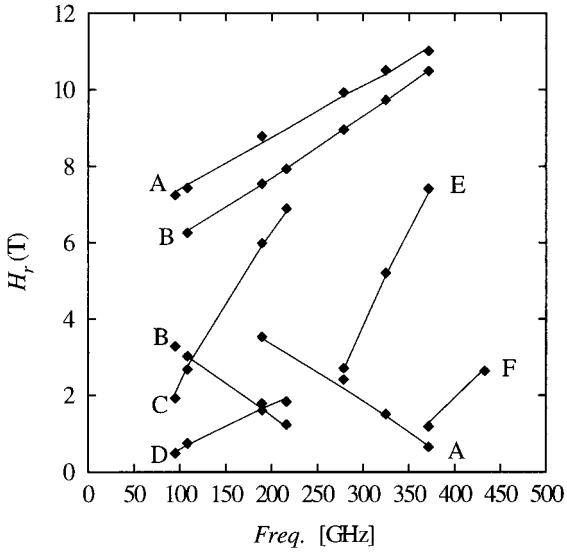

Figure 8. Resonant field vs frequency diagram for axial resonances of $[PPh_4]_2[Fe(SPh)_4]$. The experimentally observed resonances (◆) are plotted along with the resonance positions from simulations (solid lines). See the text for simulation parameters.

Z axis between the $|1^s\rangle$ and $|2^a\rangle$ energy levels. The transition $|1^a\rangle \rightarrow |1^s\rangle$ has a frequency dependence as shown by the branches marked "B" (for *H*||*Y*) and "E" (for *H*||*X*). Two of the three remaining resonances (lines C and D) each indicate the frequency dependence of transitions between the energy levels $|1^a\rangle$ and $|0'\rangle$, "C" for *H*||*X* and "D" for *H*||*Y*. The final branch (F) is only evident at the highest frequencies and indicates the frequency behavior of a resonance between the $|0'\rangle$ and $|1^a\rangle$ levels when *H*||*Y*.

The Zeeman energy splittings of Fe^{2+} along the three molecular axes were calculated and are plotted in Figure 9. In this figure, the Zeeman splitting when *H* is parallel with each of the molecular axes, *X*, *Y*, and *Z*, is plotted in a separate frame. It is very clear that the splittings of these levels are quite different along each axis and that there is a great deal of curvature in the Zeeman splittings, which indicates extensive level mixing. EPR resonances are possible at fields where the resonance condition is met ($g\beta H = h\nu$); the observed resonances at 189.83 GHz are indicated by vertical bars.

The results of the present study underscore the value of a multifrequency approach to investigate high-spin transition metal ions having large and considerably rhombic zfs tensors. Such an approach can greatly facilitate attributing observed EPR peaks to transitions between particular spin levels, as shown in Figure 8. Also, it allows one to "tune in" the spin system under study by selecting a frequency yielding maximum information on that system. This frequency strongly depends on the zfs parameters and need not be highest one available; in the case of zfs on the order of 6 cm^{-1} and high rhombicity of E/D $\gg$ 0.25, it happens to be around 190 GHz; in other systems, it will be different.

Of the two parameters characterizing the new technique of HFEPR, namely high frequency and high magnetic fields, the latter appears to have at least as much importance as high, and adjustable, frequency. By looking at Figure 9, one may conceive an extension of an X- or Q-band spectroscopy by adding a sweepable superconducting magnet to a conventional spectrometer. Several transitions would then be potentially observable at high fields, particularly near the level crossing/anticrossing regions, which are inaccessible with conventional electromagnets.

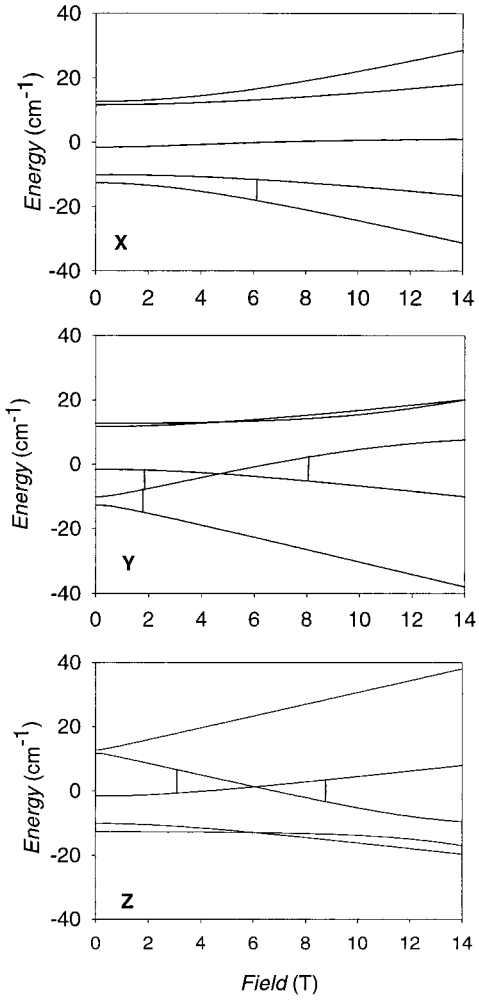

Figure 9. Plots of the energy vs field for the five energy levels arising from an $S = 2$ spin state with $g_x = g_y = 2.08$ and $g_z = 2.00$ that is split by zero-field splitting where $D = +5.84$ cm^{-1} and $E = +1.42$ cm^{-1}. The field is parallel to the molecular axis that is indicated in each frame.

Interpretation of Spin Hamiltonian Parameters. Fe^{2+} (d^6) in a tetrahedral coordination environment has an orbitally degenerate ^5E ground state.[19] The Jahn−Teller effect can lift this orbital degeneracy by either a compression or an elongation along a tetragonal axis, leading to a $^5A_1$ or a $^5B_1$ ground state, respectively. This splitting is shown in Figure 10; a $^5A_1$ ground state indicates that the d_{z^2} orbital has the "extra" electron, whereas a $^5B_1$ ground state indicates that a $d_{x^2-y^2}$ orbital has the extra electron. The origin of zero-field splitting is the spin−orbit coupling between the ground state and nearby excited electronic states.[18−20,38] The spin−orbit contribution is inversely proportional to the energy difference between the ground state and an excited state, and for this reason, the principal contributor to the zfs of a ^5E derived state is the low-lying $^5T_2$ excited state.

Perturbation relationships have been derived that relate the spin Hamiltonian (eq 1) parameters (**g**, D, E) to more fundamental parameters (λ, ρ, $10Dq$, δ) that reflect this spin−orbit interaction. The spin−orbit coupling constant is λ, ρ is the spin−spin coupling constant, Δ is the crystal field splitting between the ^5E and $^5T_2$ states ($\Delta = 10Dq$), and δ is an angle that accounts for distortions of this crystal field from simple cubic symmetry. For a $^5A_1$ ground state, these relationships are as follows:[11,23,39]

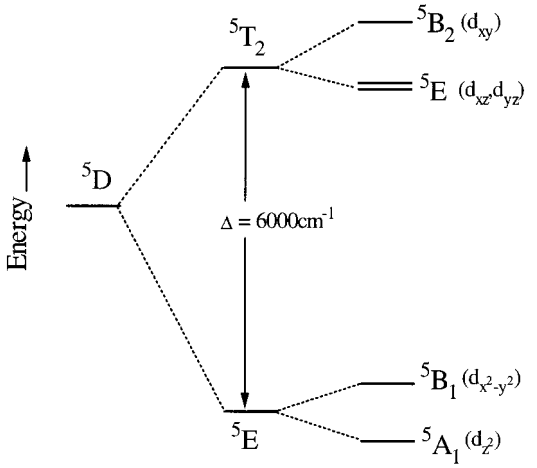

Figure 10. Ligand field splitting of a high-spin Fe^{2+} ion. The free ion in the ^5D state experiences a tetrahedral crystal field of 6000 cm^{-1} that splits the ^5D state into a ground ^5E state and an excited $^5T_2$ state. A tetragonal compression breaks the orbital degeneracies of these states, yielding the splitting pattern on the right.

$$D = -3(\rho + \lambda^2/\Delta)\cos 2\delta \quad (4a)$$

$$E = -3^{1/2}(\rho + \lambda^2/\Delta)\sin 2\delta \quad (4b)$$

$$g_x = g_e - 2(\lambda/\Delta)(\cos\delta - 3^{1/2}\sin\delta)^2 \quad (5a)$$

$$g_y = g_e - 2(\lambda/\Delta)(\cos\delta - 3^{1/2}\sin\delta)^2 \quad (5b)$$

$$g_z = g_e - 8(\lambda/\Delta)\cos^2\delta \quad (5c)$$

The ground state in this formalism is an admixture of the two lowest levels represented[11] by $\Psi = [(\cos\delta)|^5B_1\rangle + (\sin\delta)|^5A_1\rangle]$. The observation of a positive D value requires that the ground state be dominantly $^5A_1$; however, a rhombic component ($E \neq 0$) is only possible if these states mix, which is indicated by varying δ from 90°. The reduction of λ from the free ion[40] value ($\lambda_{free} = -104$ cm^{-1}) can be calculated as -80 cm^{-1}. If we take ρ as 0.95 cm^{-1} [41] and Δ as 6000 cm^{-1} [15] and use our simulated zfs parameters of $D = +5.84$ cm^{-1} and $E = +1.42$ cm^{-1}, we calculate the distortion parameter as $\delta = 100°$ from eqs 4a and 4b. This indicates that the ground state is predominantly (97%) $^5A_1$ (d_{z^2} orbital lowest), with a small component (3%) of $^5B_1$ mixed in. Furthermore, from this derived distortion δ, we calculate **g** to be ($g_x = 2.09$, $g_y = 2.06$,$g_z = 2.00$), which is in very good agreement with our simulations ($g_x = g_y = 2.08$, $g_z = 2.00$).

The same perturbation relationships may be used to estimate the zfs of Rd_{red}. The optical spectra reveal a d−d transition at 6250 cm^{-1}, which provides a good estimate for Δ, and Mössbauer data indicate that the rhombicity is $E/D = 0.28$. The distortion parameter δ may be obtained by the relationship[11] $E/D = 1/3^{1/2}(\tan 2\delta)$. This relationship indicates that $\delta = 103°$, which is quite close to the value observed for $[PPh_4]_2[Fe(SPh)_4]$. If we assume $\lambda = -80$ cm^{-1} and $\rho = 0.95$ cm^{-1}, as was done above, the zfs parameters for Rd_{red} are estimated by eqs 4a and 4b as $D = +5.3$ cm^{-1} and $E = +1.5$ cm^{-1}. This is in contrast to the results from fitting Mössbauer data, where the zfs parameters were fit as $D = +7.6$ cm^{-1} and $E = 2.1$ cm^{-1}. It

(38) Bertrand, P.; Gayda, J.-P. *Biochim. Biophys. Acta* **1988**, *954*, 347−350.
(39) Ono, K. *J. Phys. Soc. Jpn.* **1957**, *12*, 1231−1238.
(40) Figgis, B. N. *Introduction to Ligand Fields*; Interscience: New York, 1966.
(41) Pryce, M. *Phys. Rev.* **1950**, *80*, 1107−1108.

appears that the reported magnitude of D for Rd_{red} is too large for two reasons. First, D for $[PPh_4]_2[Fe(SPh)_4]$ had also been reported[42] to be a similar, large value (7.55 cm^{-1}) from Mössbauer spectra, which indicates the inaccuracy of D values resulting from those fits. Second, the observed d−d transition of Rd_{red} implies that Δ is close to 6250 cm^{-1}, which requires that $|D| < 6$ cm^{-1} within the approximation of eq 4a. It would be interesting to investigate Rd_{red} by HFEPR, to better determine the magnitude of D. HFEPR provides another tool for the analysis of the active sites of ferrous enzymes.

Conclusions

The electronic structure of the Rd_{red} model $[PPh_4]_2[Fe(SPh)_4]$ has been successfully characterized by high-frequency EPR spectroscopy on a randomly oriented sample. Multiple transitions between the non-Kramers doublets and singlet of the $S = 2$ ground state have been observed, providing direct measurement of zero-field splitting parameters and g values. The ground-state electronic properties are quite similar to those of Rd_{red}. This system is only the third $S = 2$ transition metal ion characterized by HFEPR, and this is the first time the ferrous ion has been studied by this technique. This study is a step toward the investigation of high-spin biological systems.

Acknowledgment. We thank Dr. Joe Goldsby (Florida State University) for use of a KBr press and Dr. Høgni Weihe (Odense University, Denmark) for supplying us with the EPR simulation program. M.J.K. thanks the NIH for a predoctoral fellowship (2 T32-DK07233) and the NHMFL Visitor's Program for partial funding of this research. J.K. and L.C.B. thank the NHMFL for support.

IC9910054

(42) Petrouleas, V.; Simopoulos, A.; Kostikas, A.; Coucouvanis, D. *J. Phys., Calloq.* **1976**, *37*, C6-159.